Spontaneous and inducible CD8 T cell lesions in the brain and spinal cord of HLA-DR15-positive MS PBMC humanized mice

Irini Papazian[1], Maria Kourouvani[1,2], Anastasia Dagkonaki[1], Lila Dimitrakopoulou[3], Vasileios Gouzouasis[1,4], Fotis Badounas[1,5], Nikolaos Markoglou[6], Maria Belimezi[7], Emmanouil Angelakis[7], Theodore Tselios[8], Maria Anagnostouli[6], Lesley Probert[1,*]

1. Laboratory of Molecular Genetics, Department of Immunology, Hellenic Pasteur Institute, Athens, Greece.
2. Athens International Master's Programme in Neurosciences, Department of Biology, National and Kapodistrian University of Athens, Athens, Greece.
3. Department of Hematology, Laiko General Hospital, National and Kapodistrian University of Athens, Athens, Greece.
4. Department of Molecular Biology and Genetics, Democritus University of Thrace, Alexandroupolis, Greece.
5. Transgenic Technology Unit, Hellenic Pasteur Institute, Athens, Greece.
6. Research Immunogenetics Laboratory, First Department of Neurology, Aeginition University Hospital, National and Kapodistrian University of Athens, Athens, Greece.
7. Diagnosis Department, Hellenic Pasteur Institute, Athens, Greece.
8. Department of Chemistry, University of Patras, Patras, Greece.

Keywords: Humanized mice, peripheral blood mononuclear cells, HLA-DR15 MS risk factor, multiple sclerosis, experimental autoimmune encephalomyelitis, natalizumab

* Correspondence: Lesley Probert; lesley@pasteur.gr

Summary

Autoimmune diseases of the central nervous system such as multiple sclerosis (MS) are only partially represented in current experimental models and the development of humanized immune mice is crucial for better understanding of immunopathogenesis and testing of novel therapeutics. We describe a humanized mouse model with several key MS features. Severely immunodeficient B2m-NOG mice were transplanted with peripheral blood mononuclear cells (PBMC) from MS and healthy (HI) donors and showed rapid engraftment by human T and B lymphocytes. DR13-positive MS PBMC mice developed low levels of graft versus host disease (GVHD) and no CNS inflammation. Both DR15 MS and DR15 HI mice developed spontaneous and EAE-inducible infiltration of CNS barriers and parenchyma by $CD8^+$ and $CD4^+$ T cells. DR15 MS mice uniquely developed spontaneous T cell lesions in brainstem and spinal cord grey matter, and large EAE-inducible lesions in the brain corpus callosum, with relatively low GVHD levels compared to DR15 HI mice. Main limitations of this model for further development are poor monocyte engraftment, lack of demyelination and of lymph node organization and IgG responses. These results show that PBMC humanized mice represent promising experimental tools for MS immunopathology and for testing experimental immunotherapeutics in a patient-specific approach.

47 **Introduction**

48 Multiple sclerosis (MS) is a complex chronic inflammatory demyelinating and
49 neurodegenerative disease of the central nervous system (CNS) with autoimmune
50 characteristics. Pathological hallmarks are focal plaques of immune-mediated demyelination
51 in the white matter, inflammation at CNS borders and diffuse demyelination and
52 neurodegeneration of the grey and white matter of the brain and spinal cord. Genome wide
53 association studies show that the vast majority of MS risk genes are related to immune
54 activation and function, thereby strongly supporting the role of adaptive immunity in MS
55 pathogenesis. These include the strongest MS associated genetic risk factor, human
56 leukocyte antigen (HLA) DR15 haplotype, encoded by two DRB* genes, *DRB1*15:01* (DR2b)
57 and *DRB5*01:01* (DR2a), of the MHC class II that restricts $CD4^+$ T cells (1,2). Pathological
58 analyses of autopsy tissues reveal $CD8^+$ lymphocytes and monocytes as the main CNS
59 infiltrating cells, with B cells accumulating in meningeal and perivascular spaces, and
60 relatively few infiltrating $CD4^+$ T cells (3). Studies in animal models, mainly experimental
61 autoimmune encephalomyelitis (EAE), showing that myelin-reactive T cells are both
62 necessary and sufficient to induce EAE, as well as the effectiveness of current
63 immunotherapies in MS patients that work mainly by targeting peripheral immune
64 responses, further support an autoimmune pathogenesis for MS.

65

66 EAE and MS share many clinical, immunological, and pathological similarities (4,5), but they
67 also present significant differences (6,7). One difference is the predominance of $CD8^+$ T cells
68 in MS lesions, while these cells are scarce in the CNS of EAE mice (8). In addition, the
69 inflammatory process in EAE primarily targets the spinal cord, whereas in MS it also targets
70 the brain. Moreover, while some MS drugs were discovered from research in the EAE model
71 (natalizumab, glatiramer acetate), there is a relatively low or moderate success rate of drugs
72 that showed high efficacy in both the EAE model and the human disease (9). These
73 differences infer that different pathways or mechanisms are prevalent in MS versus EAE
74 (10,11). Differences are further highlighted by recent clinical data showing the critical
75 importance of B cells to MS pathology, a cell population that does not show functional
76 participation in most EAE models (12,13). The development of animal models capable of
77 developing human immune system is crucial to the study of human immune-mediated
78 diseases such as MS, and for evaluating the safety and efficacy of human immunotherapies.

79 Most current studies with humanized mouse models use immunodeficient non-obese
80 diabetic (NOD) - severe combined immunodeficiency disorder (*scid*) mice deficient or
81 mutant for the common cytokine receptor γ-chain gene (*IL2rg)* (named NSG or NOG mice,
82 respectively) that lack B, T cells and NK cells and have defective innate immune responses
83 (14–17). These mouse strains readily engraft with human peripheral blood monocytes
84 (PBMC) without prior irradiation, as murine MHC molecules support the proliferation of
85 both $CD4^+$ and $CD8^+$ T cells, with $CD8^+$ T cells predominating. Recent variants of these strains
86 lacking MHC class I molecules (B2m) show increased CD4 to CD8 ratios and a longer time
87 window before onset of xenogeneic graft versus host disease (GVHD) and represent
88 improved strains for the study of human immune responses (18,19). Previous studies
89 showed that PBMC humanized NSG mice with cells from healthy donors are susceptible to
90 EAE, exhibiting subclinical disease, with infiltration of the brain and spinal cord by $CD4^+$ and
91 $CD8^+$ T cells, but not monocytes (20).
92
93 To investigate the potential of PBMC from MS patients to induce CNS-directed
94 immunopathology in humanized mice, we engrafted B2m-NOD/*scid*-IL2Rγ^{null} (B2m-NOG)
95 mice with PBMC from 3 human donors based on HLA-DRB1 genotype and RRMS diagnosis,
96 and monitored CNS inflammation that developed spontaneously or after immunization with
97 myelin antigens. We show that PBMC from MS and healthy (HI) donors rapidly engraft B2m-
98 NOG mice, but with marked differences towards the proportions of immune cell populations
99 engrafted and propensity to develop CNS inflammation between donors. Mice transplanted
100 with PBMC from HLA-DR15-positive MS and HI donors engrafted with human (h)$CD4^+$ and
101 $hCD8^+$ T cells and showed prominent $hCD8^+$ T cell accumulation at CNS borders and
102 infiltration of brain and spinal cord parenchyma associated with locally activated microglia
103 and astrocytes. Overall, CNS inflammation tended to be more severe in DR15 MS mice and
104 uniquely showed spontaneous $hCD8^+$ T cell lesions in the spinal cord grey matter and
105 brainstem, and prominent corpus callosum white matter lesions in mice immunized with
106 myelin peptides. Our results show that the PBMC humanized B2m-NOG mouse model
107 partially reproduces MS immunopathology and can be used to investigate human immune
108 responses towards CNS in a simple, fast, and personalized manner.
109
110

111 **Results**

112 *Reconstitution of human adaptive immune system in B2m-NOG mice engrafted with PBMC*
113 *from MS patient and HI donors*

114 Two long-term RRMS patients, one HLA-DR15-positive (DR15 MS) and one HLA-DR13-
115 positive (DR13 MS), both presenting with highly active disease following
116 immunomodulatory treatment with natalizumab, were selected as PBMC donors (Table 1).
117 An HLA-DR15-positive healthy individual (DR15 HI) was selected as a control donor. Fresh
118 blood samples were used for immunoprofiling by flow cytometry with a panel of standard
119 human immune cell marker antibodies (Supplementary Table 1A, B), for screening of plasma
120 antibody responses to viruses (Table 1; and Supplementary Table 1C for interpretation of
121 EBV results), and for the isolation of fresh PBMC. Groups of 8 B2m-NOG mice were injected
122 intravenously with freshly prepared PBMC (1 x 10^7/mouse) from each donor
123 (Supplementary Table 2, protocol 1). The transplanted mice were monitored for human
124 immune cell engraftment by flow cytometry analysis of small blood samples recovered from
125 the tail vein at different time points and all showed progressive engraftment by human
126 $CD45^+$ ($hCD45^+$) leukocytes from day 7 (Fig. 1A). At day 14 post-transplantation (dpt 14), 5
127 mice from each group were immunized for EAE using a mixture of immunodominant T cell
128 myelin peptide antigens. The PBMC donors used in this study show T cell proliferation
129 responses to myelin peptides (Table 1), as shown in a previous study (21). Non-immunized
130 mice showed steadily increasing levels of blood $hCD45^+$ leukocytes up to sacrifice at dpt 42.
131 Immunized mice showed reduced levels of blood $hCD45^+$ leukocytes following immunization
132 (Fig. 1A). Further FACS analysis showed preferential expansion of $hCD4^+$ T lymphocytes
133 compared to $hCD8^+$ T lymphocytes in blood and spleens of all mice (Fig. 1B, C), a finding
134 consistent with a previous report describing the B2m-NSG model (18).

135

136 Successful engraftment of mice by $hCD45^+$ leukocytes was confirmed in the spleen
137 recovered from non-immunized and immunized mice at sacrifice on dpt 42 (Fig. 1A). Further
138 analysis of splenocytes revealed robust engraftment of $hCD4^+$ and $hCD8^+$ T cells in all mice,
139 and of $hCD19^+$ B cells in DR13 MS PBMC mice (Fig. 1C; Supplementary Table 3). Human
140 immune cells other than T and B cells, notably monocytes, were undetectable in dpt 42
141 spleen. Analysis of cytokine production by intracellular staining showed high proportions of

142 IFN-γ-producing hCD4$^+$ and hCD8$^+$ splenocytes, and IL-17A-producing hCD4$^+$ in both
143 immunized and non-immunized mice (Fig. 1E).
144
145 To estimate the contribution of mouse myeloid cell populations in the humanized mice, we
146 analyzed peripheral blood from a parental NOD-*scid* mouse strain and wild-type C57BL/6
147 (B6) mice, non-immunized (naïve) or day 8 post-immunization (dpi 8) with CFA and
148 intraperitoneal (i.p.) injections with *Bordetella pertussis* toxin (PTx) following the EAE
149 protocol, by flow cytometry. Immature Ly6C^{hi} monocytes and Ly6G$^+$ cells are known to
150 massively expand in the periphery of wild-type B6 mice following immunization with
151 adjuvants and are critical for the development of EAE in wild-type mice (22,23). Unlike B6
152 mice, very high proportions of mouse (m) CD11b$^+$, mCD11b$^+$Ly6C^{hi} and mCD11b$^+$Ly6G$^+$
153 myeloid cells were already present in the blood of non-immunized NOD-*scid* mice, and these
154 did not increase significantly following immunization (Supplementary Table 4).
155
156 Functionality of the human immune system in B2m-NOG mice was investigated using an *ex*
157 *vivo* proliferation assay for T cell responses in splenocytes (23), and a cell-based assay for
158 anti-MOG antibody responses in plasma. Briefly, splenocytes recovered from non-
159 immunized and immunized mice at sacrifice were stimulated *ex vivo* individually with the 4
160 myelin peptides used for immunization (mMOG35-55, hMOG35-55, MOG1-20, MBP83-99).
161 T cell proliferation responses were measured using a CFSE dilution assay. Splenocytes
162 isolated from DR13 MS mice (Fig. 1D), not DR15 MS or DR15 HI mice (data not shown),
163 showed significant T cell proliferation responses to all myelin peptides, equal to control
164 splenocytes stimulated with anti-hCD3 antibody. The difference in responses between
165 donors might be explained by the significant engraftment of human B cells in DR13 MS mice,
166 which can act as antigen-presenting cells in the *ex vivo* T cell proliferation assay. Anti-hMOG
167 IgG antibody responses were not detectable in the plasma of any mice at any time point.
168
169 We next investigated whether draining lymph nodes (LN) structures could be identified in
170 the immunized mice at sacrifice. Mice lacking the common cytokine receptor γ-chain gene
171 are known to have poor lymphoid organ structure and functioning, because NK cells are
172 needed for the formation of LN inducer cells, which in turn are needed for LN organogenesis
173 (24). Nevertheless, the inguinal fat tissue from several immunized mice showed

174 accumulations of leukocytes containing mCD45- and hCD45-positive leukocytes, CD8-, CD4-
175 and CD20-positive lymphocytes by immunohistochemistry, although lacking obvious LN
176 organization (Fig. 1F). Together the results show that human T and B lymphocytes are
177 efficiently engrafted in B2m-NOG mice by PBMC from MS patients, that functional T cell
178 responses can be detected, depending upon the PBMC donor, while lack of organized LN
179 and germinal centers prevents the generation of anti-MOG IgG antibody responses.
180
181 *Human T cells accumulate at CNS borders in non-immunized DR15 MS and DR15 HI mice,*
182 *and form spontaneous parenchymal lesions in brainstem and spinal cord of DR15 MS mice*
183 For the period of the study, none of the engrafted mice showed clinical symptoms of
184 neuroinflammation or EAE using criteria commonly used for scoring EAE (21), or other
185 neurological deficits (25). Mild symptoms of GVHD, specifically fur ruffling and reduced
186 mobility (26), were recorded in few mice independent of group close to the time of sacrifice.
187 To determine whether human immune cells enter CNS tissues in PBMC humanized B2m-
188 NOG mice, we performed immunohistochemical analyses of serial sections from brain and
189 spinal cord recovered from non-immunized mice at sacrifice using marker antibodies for
190 human and mouse immune cells as well as for mouse microglia and astrocytes. To further
191 monitor GVHD development we also performed standard histological analyses of lung and
192 liver, two main tissues targets of GVHD.
193
194 DR13 MS humanized mice showed very few hCD45-positive leukocytes at CNS borders,
195 specifically meninges, and none in CNS parenchyma, so no further analysis was made (data
196 not shown). DR15 HI mice showed an accumulation of human immune cells at CNS borders,
197 particularly the meninges and some in the choroid plexus of the interventricular foramen
198 between lateral and third ventricles (Fig. 2A, C, D, arrowheads). In the brain, individual
199 hCD45-positive leukocytes were scattered throughout the parenchyma and comprised
200 mainly hCD8-positive T cells (Fig. 2C) and fewer hCD4-positive T cells (data not shown). Mild
201 activation of Iba1-positive microglia and GFAP-positive astrocytes was seen at sites of
202 immune cell accumulation at CNS borders (Fig. 2C). In spinal cord, hCD3-positive T cells
203 accumulated at borders and few individual cells infiltrated parenchyma of white and grey
204 matter (Fig. 3A, B). Sparse small T cell lesions (≥ 3 adjacent cells) were detected in the white
205 matter of the spinal cord (Fig. 3A, left panel, arrowhead). Mouse CD45-positive cells were

206 sparse at barriers, absent from parenchyma, and demyelination was not observed in the
207 brain or spinal cord of DR15 HI mice.
208
209 DR15 MS mice showed more severe pathology than HLA-DR15 HI mice, with accumulation
210 of human immune cells at CNS borders, particularly the meninges and choroid plexus of the
211 interventricular foramen between lateral and third ventricles (Fig. 2A, C, D, arrowheads),
212 widespread immune cell infiltration of the parenchyma, and small T cell lesions in the
213 brainstem and spinal cord. In the brain, hCD45-positive leukocytes comprised mainly hCD8-
214 positive T cells (Fig. 2C, arrows) and fewer hCD4-positive T cells, (data not shown). Numbers
215 of brain parenchymal hCD8-positive T cells tended to increase in the brain parenchyma of
216 DR15 MS mice compared to control HI mice, but differences were not significant due to
217 variation within the groups (Fig. 2E). Unlike control HI mice, DR15 MS mice showed
218 parenchymal T cell lesions (≥ 3 adjacent cells) in brainstem (Fig. 2A, B). Locally activated
219 Iba1-positive microglia and GFAP-positive astrocytes were observed at sites of immune cell
220 accumulation (Fig. 2C, D, arrowheads). In the spinal cord, hCD3-positive T cells accumulated
221 at borders and infiltrated both white and grey matter parenchyma (Fig. 3A). T cell lesions
222 were present in spinal cord white and grey matter (Fig. 3A, right panels, arrowheads).
223 Numbers of parenchymal hCD3-positive T cells in whole spinal cord sections tended to be
224 increased in DR15 MS mice compared to control HI mice, but differences were not
225 significant (Fig. 3C). However, unlike control HI mice, DR15 MS mice showed numerous
226 small T cell lesions in the grey matter, often close to the central canal suggesting this is a
227 main site of human T cell entry into the spinal cord grey matter (Fig. 3A, right panel,
228 arrowheads, B). Mouse CD45-positive cells were rare at barriers, absent from parenchyma,
229 and demyelination was not observed in the brain or spinal cord of DR15 MS mice.
230
231 To determine whether differences in the severity of CNS immune infiltration in the
232 immunized mice was secondary to levels of GVHD inflammation in the periphery, we
233 performed semi-quantitative analysis of H&E stained liver and lung sections, which are main
234 targets of GVHD responses (26). All mouse groups showed equal levels of inflammation in
235 both liver and lung, revealing a dissociation between peripheral GVHD and CNS
236 inflammation (Supplementary Fig 1). These results show that non-immunized DR15 MS
237 humanized mice have increased infiltration of brain and spinal cord by human T cells

238 compared to non-immunized DR15 HI mice, and uniquely develop hCD8$^+$ T cell lesions in
239 spinal cord grey matter and brainstem parenchyma.
240
241 *Immunization with myelin peptides increases T cell infiltration of CNS parenchyma and*
242 *promotes development of brain and spinal cord lesions in both DR15 MS and DR15 HI mice*
243 To further investigate whether human immune cells have the potential to induce CNS
244 immunopathology in PBMC humanized B2m-NOG mice, we immunized mice following an
245 EAE protocol using a mixture of immunodominant myelin peptides. In a previous study, we
246 found that humanized HLA-DR2b transgenic mice lacking all mouse MHCII genes required
247 greater amounts of peptide antigen to induce clinical EAE than wild-type B6 mice (21). We
248 tested several EAE protocols using wild-type B6 mice, mainly to exclude the possibility of
249 toxicity at high peptide doses. Briefly, 8-week-old female B6 mice were immunized by
250 subcutaneous (s.c.) tail-base injection of 37 µg (standard EAE protocol in B6 mice) or 200 µg
251 mMOG35-55 (protocol used in HLA-DR2b transgenic mice), or a myelin peptide antigen
252 cocktail containing 200 µg each of mMOG35-55, hMOG35-55, MOG 1-20 and MBP83-99,
253 dissolved in 100 µl saline and emulsified in an equal volume of complete Freund's adjuvant
254 (CFA), together with i.p. PTx injections. Mice receiving high dose peptide also received an
255 identical booster immunization 7 days after the first. All mice developed clinical symptoms
256 of EAE, albeit with delayed disease onset in the high peptide groups possibly due to
257 induction of T cell tolerance in B6 mice, with no evidence of increased morbidity or
258 mortality at high peptide doses (Supplementary Fig. 2). For this reason, the high-dose
259 peptide cocktail was chosen for immunization of groups of 12-14-week-old humanized B2m-
260 NOG mice on dpt 14. Mice were monitored for engraftment by human immune cells (see
261 above, and Fig. 1) and clinical symptoms at different time points, and brain and spinal cord
262 tissues were recovered at sacrifice for immunohistochemical analysis using marker
263 antibodies for human and mouse immune cells as well as for mouse microglia and
264 astrocytes. In agreement with a previous study in NSG mice humanized with PBMC from
265 healthy donors (20), none of the mice immunized with myelin antigens developed typical
266 clinical symptoms of EAE.
267
268 To investigate whether immunization increased immune cell infiltration of the brain and
269 spinal cord we performed immunohistochemical analysis of tissues recovered from the mice

270 at sacrifice at dpt 42. Immunized DR13 MS mice, like their non-immunized group, showed
271 very few hCD45-positive leukocytes at CNS borders and infiltrating spinal cord parenchyma,
272 so no further analysis was made (data not shown). Immunized DR15 HI mice, like their non-
273 immunized group, showed an accumulation of human immune cells at CNS borders,
274 particularly the meninges and choroid plexus. In the brain, individual hCD45-positive
275 leukocytes were scattered throughout the brain parenchyma and comprised mainly hCD8-
276 positive T cells (Fig. 4A, B) and fewer hCD4-positive T cells (not shown). In one of three
277 immunized mice, small T cell lesions were present in the optic tract (Fig. 4C, arrowhead).
278 Locally activated Iba1-positive microglia and GFAP-positive astrocytes were present at sites
279 of immune cell accumulation at borders and in optic tract lesions (Fig. 4C). In spinal cord,
280 hCD3-positive T cells accumulated at borders and individual cells infiltrated grey and white
281 matter (Fig. 5A), forming small T cell lesions in the white matter (Fig. 5A, B). Mouse CD45-
282 positive cells were rare at barriers, absent from parenchyma, and demyelination was not
283 observed in the brain or spinal cord of immunized DR15 HI mice.
284
285 Immunized DR15 MS mice showed prominent accumulation of human immune cells at CNS
286 borders, widespread immune cell infiltration of the parenchyma and development of T cell
287 lesions in the brain and the spinal cord (Figs. 4 and 5). Brain infiltrates comprised mainly
288 hCD8-positive T cells, and fewer hCD4-positive T cells (Fig. 4D, arrowheads). Accumulation
289 at borders and infiltration of parenchyma by hCD8- positive cells in immunized DR15 MS
290 mice was increased compared to immunized DR15 HI mice, but differences in numbers of
291 hCD8-positive T cells did not reach significance (Fig. 4E). A unique feature of immunized
292 DR15 MS mice was the presence of large T cell lesions in the corpus callosum white matter
293 (Figs. 4D and G, arrowheads), and small lesions in other brain regions (e.g. hypothalamus,
294 cortex, periventricular regions; data not shown). Locally activated Iba1-positive microglia
295 and GFAP-positive astrocytes were present at sites of immune cell entry at CNS borders and
296 in T cell lesions (Fig. 4D). In the spinal cord, like in immunized DR15 HI mice, hCD3-positive T
297 cells accumulated at borders and individual cells infiltrated grey and white matter (Fig. 5A,
298 right panels), but forming small T cell lesions only in the white matter (WM) (Fig. 5A, B).
299 Numbers of hCD3-positive T cells counted in whole spinal cord sections were equal to those
300 in immunized HLA-DR15 HI mice (Fig. 5D). Again, mCD45-positive cells were rare at barriers,

301 absent from parenchyma, and demyelination was not observed in the brain (Fig. 4G) or
302 spinal cord (Fig. 5C) of immunized DR15 MS mice.
303
304 To determine whether CNS immune infiltration in the immunized mice was secondary to
305 levels of GVHD inflammation in the periphery, we performed semi-quantitative analysis of
306 H&E stained liver and lung sections. Immunized DR13 MS mice showed the lowest levels of
307 immune cell infiltration in liver and lung, DR15 MS mice intermediate levels, and DR15 HI
308 highest levels (Supplementary Fig. 1). Results revealed an inverse relationship between
309 peripheral and CNS inflammation in the DR15 HI and MS mice, with DR15 HI mice showing
310 highest peripheral and relatively lower CNS involvement, while DR15 MS mice showed the
311 highest CNS and relatively lower peripheral inflammation. These results show that
312 immunization of DR15 HI and DR15 MS mice with myelin peptides equally induced spinal
313 cord white matter inflammatory lesions, and uniquely induced large confluent corpus
314 callosum white matter lesions in DR15 MS mice. Taken together, our results show that
315 PBMC from a DR15-positive MS patient show increased propensity to induce inflammatory
316 CNS lesions compared to PBMC from a DR13-positive MS patient or a DR15-positive healthy
317 individual.
318
319 **Discussion**
320 Here we show that PBMC from RRMS and healthy donors with different HLA genotypes have
321 the potential to efficiently engraft B2m-NOG mice with human T and B lymphocytes and to
322 induce sub-clinical CNS inflammation dominated by $hCD8^+$ T cells in the brain and the spinal
323 cord. Specifically, mice engrafted with PBMC from DR15-positive MS and healthy donors,
324 and not from a DR13-positive MS donor, showed spontaneous brain and spinal cord
325 infiltration by $hCD8^+$ and $hCD4^+$ T cells which tended to be more severe in DR15 MS mice.
326 DR15 MS mice uniquely developed prominent T cell lesions in several brain regions including
327 the corpus callosum following immunization with myelin peptides using an EAE protocol. T
328 cell lesions were associated with locally activated microglia and astrocytes, but notably
329 lacked infiltrating monocytes and demyelination, and did not lead to clinical symptoms of
330 EAE or other neurological defects.
331

332 PBMC humanized B2m-NOG mice developed several hallmark features of MS that are not
333 readily reproduced in conventional animal models, such as EAE. First, brain immune
334 infiltrates in DR15 MS engrafted mice were enriched for hCD8$^+$ over hCD4$^+$ T cells, even
335 though the B2m-NOG model is characterized by increased engraftment of CD4$^+$ over CD8$^+$ T
336 cells (18) (Figure 1B). The preferential infiltration of the CNS parenchyma by CD8$^+$ T cells,
337 and the presence of inflammatory lesions in the brain white matter in our model are both
338 features of MS (3,8,27). Second, T cell lesions and locally activated microglia and astrocytes,
339 were observed in brain white matter regions, particularly the corpus callosum. Lesions in
340 the corpus callosum are important findings in MRI of MS patients and are correlated with
341 cognitive problems as well as disability in the upper limbs (28). Third, human leukocytes
342 were concentrated on the meninges and choroid plexus, notably in the interventricular
343 foramen connecting the lateral and third ventricles. The choroid plexus is an important
344 immunological site for immune surveillance and a site of CD8+ T cell and granulocyte
345 involvement in progressive MS (29).
346
347 Nevertheless, MS is a complex disease and immunopathology was only partially reproduced
348 in the brain and the spinal cord of PBMC humanized B2m-NOG mice. Parenchymal lesions
349 contained both hCD4$^+$ and hCD8$^+$ T cells associated with locally activated microglia and
350 astrocytes, but there was poor engraftment by human monocytes in the blood, spleens or
351 CNS of both immunized and non-immunized B2m-NOG mice. Blood myeloid cells are short-
352 lived and constantly renewed by the bone marrow, so that human myeloid cells are nearly
353 absent in the commonly used PBMC-NSG model (18). In contrast, mouse CD45$^+$ cells
354 comprising very high proportions of CD11b$^+$ myeloid cells, Ly6C^{hi} monocytes and Ly6G$^+$ cells,
355 were present in the blood of immunized and non-immunized NOD-*scid* mice, which are a
356 parental strain for B2m-NOG mice. Nevertheless, mouse CD45$^+$ myeloid cells did not
357 infiltrate the CNS of the humanized mice, even after EAE induction. The absence of CNS-
358 infiltrating monocytes in the PBMC humanized B2m-NOG mice NOG mice likely underlies
359 the absence of clinical symptoms and demyelination in this system. Our results are
360 consistent with a previous study in which NSG mice were humanized with PBMC from
361 healthy donors and immunized for EAE (20). In that study, mice developed CNS
362 inflammation with infiltrating CD4$^+$ and CD8$^+$ T cells but did not show clinical symptoms or
363 demyelination (20). CNS-infiltrating Ly6C^{hi}CCR2$^+$ monocytes, which differentiate into

364 inflammatory macrophages locally in the CNS after being activated by T cells, are critical
365 effector cells in EAE (22,30). These cells are massively recruited into the periphery from the
366 bone marrow following immunization (23), and are likely to compete for space with
367 engrafted human immune cells following EAE induction. The use of immunodeficient
368 NOG/NSG models expressing human transgenes that would enhance the engraftment of
369 human monocytes, such as GM-CSF, or facilitate communication of human T cells with
370 mouse inflammatory monocytes (31,32), should allow a more comprehensive modeling of
371 MS immunopathology in humanized mice.
372
373 Another limitation for MS modeling in the B2m-NOG mice used in this study is the poor LN
374 structure and functioning that results from depletion of the common cytokine receptor γ-
375 chain gene (24). This deficiency was confirmed in this study by the absence of organized LN
376 and germinal follicles, and of anti-MOG IgG antibodies in the PBMC humanized B2m-NOG
377 mice immunized for EAE. Again, further development of available immunodeficient mouse
378 strains to promote LN organogenesis will be an important step for modeling MS
379 immunopathology in mice. In a previous study, NSG mice injected directly in the CNS with
380 CSF cells from MS patients (33) developed clinical symptoms, immune infiltration of the CNS
381 and demyelination, although differences in the route of administration of the transplanted
382 cells might explain the differences between our study and that of others (20).

383 Our observation that mice engrafted with PBMC from a DR15-positive active RRMS patient
384 showed both spontaneous and EAE-inducible T cell lesions in the brainstem and spinal cord
385 is highly relevant in the context of previous data concerning this haplotype. HLA-DR2 has
386 long been associated with MS (34), with the DR15 haplotype being linked to earlier disease
387 onset (1,35). MHCII molecules present antigens to $CD4^+$ T cells, and DR15 is strongly
388 associated with the autoproliferation of peripheral $CD4^+$ T cells in MS patients (36). T cell
389 autoproliferation is mediated by memory B cells in a HLA-DR-dependent manner, and the
390 autoproliferating T cells are increased in MS patients treated with natalizumab and enriched
391 for brain-homing T cells (37). In a recent study with humanized NSG mice, $CD34^+$
392 hematopoietic progenitor cells (HSC) from DR15-positive donors induced higher peripheral T
393 cell responses and alloreactivity compared to HSC from DR15-negative donors, and
394 increased $CD8^+$ T cell responses after Epstein-Barr virus (EBV) infection (38). There is now

395 strong evidence that EBV infection plays a major role in MS pathogenesis (39), acting
396 synergistically with DR15 to increase the likelihood of developing MS (34). DR15 individuals
397 with specific antibody reactivity to EBNA1 (amino acid 385–420) have 24-fold increased risk
398 for MS (40). Anti-EBNA-1 antibodies present high homology and react with several CNS
399 antigens, such as αB-crystallin, MBP, anoctamin 2 and more recently glial cell adhesion
400 molecule (41–44). In our study, the DR15 MS and HI donors were both positive for IgG and
401 IgM anti-EBNA-1 antibodies, which can be a sign of autoimmune disease, whereas the DR13
402 MS patient was positive for IgG anti-EA (early antigen) antibodies, which indicates either
403 primary EBV infection or possible reactivation (Table 1, and Supplementary Table 1C for
404 interpretation). In the PBMC humanized mice, we only found immune system infiltration
405 and brain lesions with the DR15 MS and DR15 HI donors and not with the DR13 MS donor.
406 This could be indicative of the presence of autoproliferating and brain-homing $CD4^+$ and
407 $CD8^+$ T lymphocytes in the blood of the DR15 MS and HI donors, particularly following
408 treatment with natalizumab, prior to transplantation in B2m-NOD mice, increasing the
409 likelihood of cross-reactivation upon encounter of similar mouse CNS antigens.
410 Nevertheless, positive correlations between the DR15 haplotype, T cell autoproliferation,
411 EBV and the development of brain lesions in humanized mice remain to be formally tested
412 in a larger study using greater numbers of DR15-positive MS donors against DR15 negative
413 MS and DR15-positive healthy controls, together with the measurement of basal levels of T
414 cell proliferation in the peripheral blood of the PBMC donors.
415
416 In summary, PBMC humanized B2m-NOG mice show partial representation of MS
417 immunopathology that is not reproduced in conventional animal models such as EAE,
418 particularly the development of $hCD8^+$ lesions in the grey and white matter of the brain and
419 spinal cord. New immunodeficient mouse strains developed to promote human monocyte
420 engraftment and the development of organized LN therefore hold great promise for
421 comprehensive modelling of MS immunopathology. An important outcome of this study is
422 that PBMC humanized B2m-NOG mice highlight the variability between the different human
423 PBMC donors, and therefore represent valuable research tools for generating personalized
424 immune models for drug screening.
425
426 **Materials & Methods**

427 **MS patients and healthy subjects**

428 Blood donors were selected from a Hellenic MS patient cohort attending the MS outpatient
429 clinic at Aeginition University Hospital of the National and Kapodistrian University of Athens
430 (NKUA) School of Medicine, supervised by Dr. Maria Anagnostouli and genotyped for the
431 HLA-DRB1 allele, at the Research Immunogenetics Laboratory, of the same Hospital, as
432 previously described (21) (Table 1). Two patients with long-term RRMS recently presenting
433 with highly active disease since the last dose of immunomodulatory therapy (natalizumab)
434 were selected. Natalizumab treatment was chosen as a criteria for this study because it
435 blocks lymphocyte migration to the brain, thereby increasing circulating T and B
436 lymphocytes (45). One patient was DR15-positive (DR15 MS), the other DR13-positive (DR13
437 MS). The DR13-positive patient additionally received cortisone treatment 1 month prior to
438 sampling because of high disease activity. A healthy DR15-matched healthy individual (DR15
439 HI) was selected as control. Donor characteristics, including viral infections and EBV status
440 are listed in Table 1. Blood samples were obtained from MS patients and healthy individuals
441 under signed informed consent in accordance with the Declaration of Helsinki and approval
442 from the Institutional Ethics Committee of Aeginition Hospital, NKUA (Protocol No:
443 7BSH46Y8N2-B66, 13/05/2015).

444 **PBMC isolation**

445 Fresh peripheral blood (50 ml) was collected in EDTA-treated polypropylene tubes and
446 PBMC were isolated under Ficoll-Histopaque®-1077 gradient centrifugation (Sigma-Aldrich).
447 Buffy coats containing blood leukocytes were washed with 2% FBS in PBS. Erythrocytes were
448 removed using ACK erythrocyte lysis buffer (BioLegend) and leukocytes were washed with
449 2% FBS in PBS. Before transfer of PBMC into mice, we compared several protocols for
450 preparation of human PBMC using blood from a healthy individual, specifically, 1) PBMC
451 isolated from fresh blood on the day of transfer, 2) PBMC isolated from blood after 3 days'
452 storage at 4°C, 3) PBMC cultured for 24 h in complete RPMI-1640 after snap freezing of
453 fresh PBMC and thawing. Cell viability and analysis of immune cell populations by flow
454 cytometry showed that freshly isolated PBMC gave the best results and were used for
455 transfer in this study (Supplementary Table 2).

456

457 **EBV antibody responses in human blood**

458 Blood plasma from the DR13 MS, DR15 MS and DR15 HI donors was analyzed for EBV
459 antibody responses using the following ELISA tests: ELISA-VIDITEST anti-VCA EBV IgG (ODZ-
460 265), ELISA-VIDITEST anti-EA (D) EBV IgG (ODZ-006), ELISA-VIDITEST anti-EBNA-1 EBV IgM
461 (ODZ-002) and ELISA-VIDITEST anti-EBNA-1 EBV IgG (ODZ-001) (Vidia). Standardized criteria
462 for the clinical interpretation of EBV antibody responses are shown in Supplementary Table
463 1C.
464
465 **Mice**
466 Ten-to-twelve-week-old female immunodeficient B2m-NOD/Shi - *scid IL2rg*^{null} (B2m-NOG)
467 mice (stock number 14957-F: NOD.Cg-B2m<em1Tac> Prkdc<scid>Il2rg<tm1Sug>JicTac;
468 Taconic Biosciences) were used for transfer of freshly isolated human PBMC. These mice
469 lack mature T, B, and NK cells and lack MHC class I molecules. Previous studies show that an
470 equivalent mouse strain, *NOD.Cg-Prkdc*^{scid}*Il2rg*^{tm1Wjl}*B2m*^{tm1Unc}*/Sz* (NSG β2m^{null}; The Jackson
471 laboratory) facilitates the engraftment of CD4^{+} over CD8^{+} T cells and exhibits delayed onset
472 of graft versus host disease (17,18). NOD.CB17-Prkdc scid/NCrHsd (Envigo) were used for
473 investigation of peripheral mouse myeloid cell populations in a related severely
474 immunodeficient mouse strain by flow cytometry.

475 Mice were transplanted via tail vein injection with 10x10^{6} PBMC in 200 μL PBS on the same
476 day as cell isolation from fresh peripheral human blood. Mice were assessed daily for
477 symptoms of GVHD, such as fur ruffling, hunched posture, reduced mobility and tachypnea
478 (26), as well as for any spontaneous neurological deficits (25).

479 All experiments were performed under sterile conditions in the Department of Animal
480 Models for Biomedical Research of the Hellenic Pasteur Institute. Mice were housed in a
481 specific pathogen-free facility in microisolator cages and given *ad libitum* UV-sterilized
482 standard chow, acidified water and gels for hydration. The experiments complied with
483 ARRIVE guidelines and were in accordance with the local Ethical Committee guidelines on
484 the use of experimental animals at the Hellenic Pasteur Institute, were approved by the
485 national authorities and complied to EU Directive 2010/63/EU for animal experiments.

486 **Immunization with myelin peptides**

487 Peptides MBP83-99, MOG1-20, and mMOG35-55 and hMOG35-55 (S42 in mMOG, P42 in
488 hMOG), were synthesized as previously described (46). In a previous study, we found that
489 humanized HLA-DR2b transgenic mice lacking all mouse MHCII genes required greater
490 amounts of peptide antigen to induce clinical EAE than wild-type B6 mice (21). Due to
491 limited numbers of B2m-NOG mice available for this study, several EAE protocols were first
492 tested using wild-type B6 mice, mainly to exclude the possibility of toxicity at high peptide
493 doses. Briefly, 8-week-old female B6 mice were immunized by subcutaneous (s.c.) tail-base
494 injection of 37 µg or 200 µg mMOG35-55, or a myelin peptide antigen cocktail containing
495 200 µg each of mMOG35-55, hMOG35-55, MOG1-20 and MBP83-99, dissolved in 100 µl
496 saline and emulsified in an equal volume of Freund's complete adjuvant (FCA) (Sigma-
497 Aldrich). FCA was supplemented with 400 µg/injection of H37Ra *Mycobacterium*
498 *tuberculosis* (Difco). All mice, except those immunized using the standard protocol (37 µg
499 mMOG35-55), received an identical boost immunization 7 days later. The immunized mice
500 also received intraperitoneal (i.p.) injections of 200 ng of *Bordetella pertussis* toxin (PTx)
501 (Sigma-Aldrich) at the time of each immunization and 48 h later. All mice developed clinical
502 symptoms of EAE with no evidence of increased morbidity or mortality at high peptide
503 doses. For this reason, the high-dose peptide cocktail was chosen for immunization of
504 groups of 12-14-week-old PBMC humanized B2m-NOG mice on dpt 14. Mice were
505 monitored daily for the clinical symptoms of EAE according to criteria commonly used for
506 scoring EAE: 0, normal; 1, limp tail; 2, hind limb weakness; 3, hind limb paralysis; 4, forelimb
507 paralysis; 5, moribund or dead (0.5 gradations represent intermediate scores) (21). Mice
508 were also monitored for signs of other neurological deficits (25).
509
510 **MOG antibody responses in PBMC humanized mouse blood**
511 Peripheral blood was collected from immunized and non-immunized mice at sacrifice on dpt
512 42, and sera collected for analysis of antibody responses. Samples were screened for IgG
513 antibodies against MOG, using indirect immunofluorescence assays (IFA). Sera were
514 analyzed at a starting dilution of 1:10, on EU 90 cells transfected with MOG protein and on
515 EU 90 control transfected cells, according to the manufacturer instructions (Euroimmun,
516 Lubeck, Germany). Visualization and evaluation of IFA results were performed under a
517 fluorescence microscope (Zeiss, Axioskop 40).
518

519 **Flow cytometry**

520 Fresh peripheral blood samples from the MS and HI donors were analyzed by FACS using a
521 panel of immune cell marker antibodies. To monitor immune cell populations, 3 ml fresh
522 peripheral blood was collected in EDTA tubes and a 100 µl aliquot was used for flow
523 cytometry. Erythrocyte lysis was achieved with with Quicklysis™ (Cytognos) for 25 min. Cells
524 were washed and incubated with an antibody mixture for human immune cell markers BV-
525 510-hCD45 (clone 2D1), APC-Cyanine 7-hCD3 (clone HIT3a), PE-Cyanine 7-hCD4 (clone
526 A161A1), PerCP-hCD8 (clone SK1), PE-hCD19 (clone 4G7), FITC-hCD56 (clone 5.1H11), APC-
527 hCD66b (clone G1OF5), BV-421-hCD14 (clone HCD14) (all from Biolegend), for 30 min at 4 °C
528 (Supplementary Table 1A). To monitor engraftment of human immune cells in B2m-NOG
529 mice, peripheral blood was collected in heparin tubes from the tail vein at dpt 7, 13 and 42.
530 Erythrocyte lysis and incubation with antibody mixture was performed as for fresh human
531 blood above, except that the APC-hCD66b antibody was replaced by mouse APC-CD45
532 (clone 30-F11) (Biolegend) (Supplementary Table 1A). Data was acquired with
533 FACSCelesta™ or FACSCanto™ II cytometer and analyzed with FACSDiva™ (BD) and FlowJo
534 software (Tree Star, Inc.).

535 For intracellular staining of IFN-γ, splenocytes were isolated at sacrifice at dpt 42 as
536 described above, and cells were stimulated with phorbol 12-myristate 13 acetate (PMA) (20
537 ng/ml, Sigma-Aldrich) and ionomycin (1µg/ml, Sigma-Aldrich) and treated with brefeldin-A
538 (5µg/ml, Sigma-Aldrich) for 3 h at 37°C/5% CO2 in order to disrupt Golgi-mediated
539 transport. Cells were fixed with 2% PFA in FBS, permeabilized using 0.5% wt/vol saponin,
540 and stained with fluorochrome-conjugated antibodies for APC-CD4 (clone RPA-T4, BD
541 Biosciences), CD8-PerCP (clone SK1, Biolegend), and PE-IFN-γ (clone B27; BD Biosciences)
542 and PE-IL-17A (clone eBio64DEC17, eBioscience). Data acquisition was performed using a
543 FACSCalibur™ cytometer and analyzed with FlowJo software (Tree Star, Inc.).

544

545 **T cell proliferation assay**

546 Spleens were isolated at sacrifice and homogenized in RPMI (Invitrogen Life Technologies)
547 containing 10% heat-inactivated FCS. To obtain single cell suspensions, the washed
548 homogenate was passed through a 70 µm cell strainer and erythrocyte lysis was performed
549 with Gey's erythrocyte lysis buffer for 5 min. The reaction was stopped with RPMI 1640/FCS.
550 Washed splenocytes at a concentration of 10^7 cells/mL in PBS were incubated with 5 µM

551 carboxylfluorescein succimidyl ester (CFSE, V12883, Thermofisher) for 15 min at 37°C. Cells
552 were washed and PBS/2% FCS was applied for 30 min at 37°C to stop the reaction. Cells
553 were washed and resuspended in RPMI 1640/FCS with 50 µM 2-mercaptoethanol (Sigma-
554 Aldrich) at concentration of 10^6 cells/ml. The cells were stimulated with in triplicates in
555 round-bottom 96-well plates with a myelin peptide antigen cocktail containing 30 µg/ml
556 each mMOG35-55, hMOG35-55, MOG1-20 and MBP83-99 for 120 h. Negative control cells
557 were incubated with medium only, and positive control cells were incubated in plates
558 coated with anti-CD3 (1µg/ml) (clone HIT3a, BD Biosciences). Results were expressed as cell
559 division index which is the ratio of %$CFSE^{low}$ splenocytes (proliferating splenocytes) cultured
560 with peptides or anti-CD3 to the of %$CFSE^{low}$ splenocytes cultured with medium only. Data
561 acquisition was performed using a FACSCalibur™ cytometer and analyzed with FlowJo
562 software (Tree Star, Inc.)
563
564 **Histopathology and Immunohistochemistry**
565 Mice were transcardially perfused with ice-cold PBS at sacrifice on dpt 42 by carbon dioxide
566 inhalation. Brains, spinal cords and peripheral tissues (including lung, liver and inguinal fat
567 tissue) were dissected and post-fixed in 4% paraformaldehyde fixative (PFA) overnight at
568 4°C. Tissues were embedded in paraffin and 5µm sections and used for
569 immunohistochemistry and histopathology. Inflammation in peripheral tissues was
570 visualized by haematoxylin and eosin (H&E) using standard techniques. Immune cell
571 infiltration and inflammation of brain and spinal cord was visualized by
572 immunohistochemistry using antibodies specific for hCD45, hCD4, hCD8, mCD45, and mouse
573 Iba1 and GFAP followed by biotinylated secondary Abs, horseradish peroxidase-labeled
574 avidin-biotin complex, and signal development using 3'3'-diaminobenzidine. Nuclei were
575 counterstained with hematoxylin. Images were captured with an Olympus DP71 microscope
576 digital camera using cell^A imaging software (Soft Imaging System GmbH). High resolution
577 immunofluorescence imaging was performed by confocal microscopy using paraffin sections
578 immunostained with marker antibodies for myelin (MBP), microglia (Iba1) followed by anti-
579 rat CF-647- (Biotrium) and anti-rabbit AlexaFluor 568- (Invitrogen) labelled secondary
580 antibodies, respectively. Nuclei were counterstained with DAPI. A Leica TCS SP8 confocal
581 microscope was used to acquire fluorescent images.
582

583 **Statistical Analysis**

584 Data were processed using Microsoft Excel, and statistical analysis was performed with
585 Graphpad Prism 8. Figures were made using Adobe Illustrator V24.3 Data was analyzed with
586 Student's t test and results are presented as means ± SEM. Results were considered
587 statistically significant when $p \leq 0.05$. Graphical abstract was created using BioRender.com

588 **Data availability statement**

589 The raw data supporting the conclusions of this manuscript will be made available by the
590 authors, without undue reservation, to any qualified researcher.

591

592 **Conflict of interest statement**

593 The authors report no conflict of interest.

594

595 **Ethics approvals**

596 The studies involving human participants were reviewed and approved by the Scientific
597 Committee of Aeginition Hospital, National and Kapodistrian University of Athens, Greece.
598 Licence 283/13-05-2015ADA: 7BΣH46Y8N2-B66. The patients/participants provided their
599 written informed consent to participate in this study. The animal study was reviewed and
600 approved by Committee for Evaluation of Experimental Procedures, Department of
601 Experimental Animal Models, Hellenic Pasteur Institute (Presided by Dr P Andriopoulos
602 pandriopoulos@patt.gov.grfor the Hellenic Republic, General Secretariat for Agricultural
603 Economy, Veterinary and Licenses). Licence number 770851/27-11-2019.

604

605 **Patient consent statement**

606 Written informed consent was obtained from the human individual(s) for the publication of
607 any potentially identifiable images or data included in this article.

608

609 **Authors contributions**

610 IP designed, set-up and performed experimental protocols for PBMC preparation and
611 humanization of B2m-NOG mice, monitored mice for clinical symptoms and performed
612 immunohistochemical analysis of CNS tissues, analysed results and prepared figures; MK
613 performed quantitative immunohistochemical analysis of CNS tissues, analysed results and

614 prepared figures; AD designed and performed EAE experiments, monitored mice for clinical
615 symptoms, performed immunohistochemistry of LN tissues and FACS analyses of humanized
616 mice, analysed results and prepared figures; LD designed human FACS antibody panel,
617 performed analyses of human and mouse blood and analysed results; VG performed FACS
618 analysis and EBV ELISA on fresh human donor blood samples; NM collected and co-
619 ordinated delivery of human donor blood samples; FB performed histological analysis of
620 peripheral humanized mouse tissues and evaluated GVHD; MB and MA designed and
621 performed cell-based anti-MOG antibody assays; TT designed, synthesized, purified and
622 characterized myelin peptide analogues; MA performed HLA genotyping, selected patients
623 for this study, and supervised Hellenic MS patient cohort; LP was responsible for overall
624 experimental design and management of project, analysed and interpreted data, wrote
625 paper. All authors contributed to the article, edited, and approved the submitted version.
626

627 **Funding**
628 This research was co-financed by European Union and Greek national funds by The
629 Management and Implementation Authority for Research, Technological Development and
630 Innovation Actions (MIA-RTDI/ EYDE-ETAK) of the Hellenic Ministry of Development and
631 Investments, through the Operational Program Competitiveness, Entrepreneurship and
632 Innovation, under the call RESEARCH – CREATE – INNOVATE (project code T1EDK-01859;
633 acronym AKESO). Research was also supported by the Hellenic General Secretariat for
634 Research and Innovation (G.S.R.I.) Flagship Action for Neurodegenerative Diseases on the
635 basis of Personalized Medicine (Project code 2018ΣΕ01300001, acronym EDIA-N).
636

637 **Acknowledgements**
638 We wish to thank Ivan Gladwyn-Ng and Dimitri Gimnopoulos at Taconic Biosciences for
639 providing B2m-NOG mice and expert scientific support, Konstantinos Kambas, Katerina
640 Nanou and George Kollias for support with the flow cytometry analyses, and Maria Avloniti
641 for contributing material. We especially thank Dr Eirini Fragkiadaki, and members of the
642 Department of Experimental Animals for Biomedical Research of HPI for their help and
643 expert support in maintenance and handling of the B2m-NOG mice during these
644 experiments.

645 **References**

646 1. International Multiple Sclerosis Genetics C, Wellcome Trust Case Control C, Sawcer S,
647 Hellenthal G, Pirinen M, Spencer CC, et al. Genetic risk and a primary role for cell-
648 mediated immune mechanisms in multiple sclerosis. Nature [Internet].
649 2011;476(7359):214–9. Available from:
650 http://www.ncbi.nlm.nih.gov/pubmed/21833088
651 2. Beecham AH, Patsopoulos NA, Xifara DK, Davis MF, Kemppinen A, Cotsapas C, et al.
652 Analysis of immune-related loci identifies 48 new susceptibility variants for multiple
653 sclerosis. 2013;45(11):1353–60.
654 3. Lassmann H. The changing concepts in the neuropathology of acquired demyelinating
655 central nervous system disorders. Curr Opin Neurol. 2019/03/21. 2019;32(3):313–9.
656 4. Regen T, Waisman A. Modeling a complex disease: Multiple sclerosis-Update 2020.
657 Adv Immunol. 2021;149:25–34.
658 5. Schreiner B, Heppner FL, Becher B. Modeling multiple sclerosis in laboratory animals.
659 Semin Immunopathol. 2009 Nov;31(4):479–95.
660 6. Attfield KE, Dendrou CA, Fugger L. Bridging the gap from genetic association to
661 functional understanding: the next generation of mouse models of multiple sclerosis.
662 Immunol Rev. 2012 Jul;248(1):10–22.
663 7. Lassmann H, Bradl M. Multiple sclerosis: experimental models and reality. Acta
664 Neuropathol. 2016/10/22. 2017;133(2):223–44.
665 8. Babbe H, Roers A, Waisman A, Lassmann H, Goebels N, Hohlfeld R, et al. Clonal
666 expansions of CD8(+) T cells dominate the T cell infiltrate in active multiple sclerosis
667 lesions as shown by micromanipulation and single cell polymerase chain reaction. J
668 Exp Med. 2000 Aug;192(3):393–404.
669 9. Wiendl H, Hohlfeld R. Multiple sclerosis therapeutics: unexpected outcomes clouding
670 undisputed successes. Neurology [Internet]. 2009;72(11):1008–15. Available from:
671 http://www.ncbi.nlm.nih.gov/pubmed/19289741
672 10. Wekerle H, Flügel A, Fugger L, Schett G, Serreze D. Autoimmunity's next top models.
673 Nat Med. 2012;18(1):66–70.
674 11. Mestas J, Hughes CCW. Of mice and not men: differences between mouse and human
675 immunology. J Immunol. 2004 Mar;172(5):2731–8.
676 12. Hauser SL, Bar-Or A, Comi G, Giovannoni G, Hartung H-P, Hemmer B, et al.

677 Ocrelizumab versus Interferon Beta-1a in Relapsing Multiple Sclerosis. N Engl J Med.
678 2017 Jan;376(3):221–34.
679 13. Li R, Bar-Or A. The Multiple Roles of B Cells in Multiple Sclerosis and Their
680 Implications in Multiple Sclerosis Therapies. Cold Spring Harb Perspect Med. 2019
681 Apr;9(4).
682 14. Allen TM, Brehm MA, Bridges S, Ferguson S, Kumar P, Mirochnitchenko O, et al.
683 Humanized immune system mouse models: progress, challenges and opportunities.
684 Vol. 20, Nature immunology. United States; 2019. p. 770–4.
685 15. Nagatani M, Kodera T, Suzuki D, Igura S, Fukunaga Y, Kanemitsu H, et al. Comparison
686 of biological features between severely immuno-deficient NOD/Shi-scid Il2rg(null)
687 and NOD/LtSz-scid Il2rg(null) mice. Exp Anim. 2019 Nov;68(4):471–82.
688 16. Willinger T, Rongvaux A, Takizawa H, Yancopoulos GD, Valenzuela DM, Murphy AJ, et
689 al. Human IL-3/GM-CSF knock-in mice support human alveolar macrophage
690 development and human immune responses in the lung. Proc Natl Acad Sci U S A.
691 2011 Feb;108(6):2390–5.
692 17. Morillon YM 2nd, Sabzevari A, Schlom J, Greiner JW. The Development of Next-
693 generation PBMC Humanized Mice for Preclinical Investigation of Cancer
694 Immunotherapeutic Agents. Anticancer Res. 2020 Oct;40(10):5329–41.
695 18. King MA, Covassin L, Brehm MA, Racki W, Pearson T, Leif J, et al. Human peripheral
696 blood leucocyte non-obese diabetic-severe combined immunodeficiency interleukin-
697 2 receptor gamma chain gene mouse model of xenogeneic graft-versus-host-like
698 disease and the role of host major histocompatibility complex. Clin Exp Immunol.
699 2009 Jul;157(1):104–18.
700 19. Morillon YMI, Smalley Rumfield C, Pellom ST, Sabzevari A, Roller NT, Horn LA, et al.
701 The Use of a Humanized NSG-β2m(-/-) Model for Investigation of Immune and Anti-
702 tumor Effects Mediated by the Bifunctional Immunotherapeutic Bintrafusp Alfa. Front
703 Oncol. 2020;10:549.
704 20. Zayoud M, El Malki K, Frauenknecht K, Trinschek B, Kloos L, Karram K, et al. Subclinical
705 CNS inflammation as response to a myelin antigen in humanized mice. J
706 neuroimmune Pharmacol Off J Soc NeuroImmune Pharmacol. 2013 Sep;8(4):1037–
707 47.
708 21. Dagkonaki A, Avloniti M, Evangelidou M, Papazian I, Kanistras I, Tseveleki V, et al.

709 Mannan-MOG35-55 Reverses Experimental Autoimmune Encephalomyelitis, Inducing
710 a Peripheral Type 2 Myeloid Response, Reducing CNS Inflammation, and Preserving
711 Axons in Spinal Cord Lesions. Front Immunol. 2020;11:575451.
712 22. King IL, Dickendesher TL, Segal BM. Circulating Ly-6C+ myeloid precursors migrate to
713 the CNS and play a pathogenic role during autoimmune demyelinating disease.
714 Blood. 2009 Apr;113(14):3190–7.
715 23. Dagkonaki A, Papalambrou A, Avloniti M, Gkika A, Evangelidou M, Androutsou M-E, et
716 al. Maturation of circulating Ly6C(hi)CCR2(+) monocytes by mannan-MOG induces
717 antigen-specific tolerance and reverses autoimmune encephalomyelitis. Front
718 Immunol. 2022;13:972003.
719 24. Mebius RE. Organogenesis of lymphoid tissues. Nat Rev Immunol. 2003 Apr;3(4):292–
720 303.
721 25. Guyenet SJ, Furrer SA, Damian VM, Baughan TD, La Spada AR, Garden GA. A simple
722 composite phenotype scoring system for evaluating mouse models of cerebellar
723 ataxia. J Vis Exp. 2010 May;(39).
724 26. Cooke KR, Kobzik L, Martin TR, Brewer J, Delmonte JJ, Crawford JM, et al. An
725 experimental model of idiopathic pneumonia syndrome after bone marrow
726 transplantation: I. The roles of minor H antigens and endotoxin. Blood. 1996
727 Oct;88(8):3230–9.
728 27. Wagner CA, Roqué PJ, Mileur TR, Liggitt D, Goverman JM. Myelin-specific CD8+ T cells
729 exacerbate brain inflammation in CNS autoimmunity. J Clin Invest. 2020
730 Jan;130(1):203–13.
731 28. Ozturk A, Smith SA, Gordon-Lipkin EM, Harrison DM, Shiee N, Pham DL, et al. MRI of
732 the corpus callosum in multiple sclerosis: association with disability. Mult Scler. 2010
733 Feb;16(2):166–77.
734 29. Rodríguez-Lorenzo S, Konings J, van der Pol S, Kamermans A, Amor S, van Horssen J,
735 et al. Inflammation of the choroid plexus in progressive multiple sclerosis:
736 accumulation of granulocytes and T cells. Acta Neuropathol Commun. 2020
737 Feb;8(1):9.
738 30. Ajami B, Bennett JL, Krieger C, McNagny KM, Rossi FM V. Infiltrating monocytes
739 trigger EAE progression, but do not contribute to the resident microglia pool. Nat
740 Neurosci. 2011 Jul;14(9):1142–9.

741 31. Codarri L, Greter M, Becher B. Communication between pathogenic T cells and
742 myeloid cells in neuroinflammatory disease. Trends Immunol. 2013 Mar;34(3):114–9.
743 32. El-Behi M, Ciric B, Dai H, Yan Y, Cullimore M, Safavi F, et al. The encephalitogenicity of
744 T(H)17 cells is dependent on IL-1- and IL-23-induced production of the cytokine GM-
745 CSF. Nat Immunol. 2011 Jun;12(6):568–75.
746 33. Saeki Y, Mima T, Sakoda S, Fujimura H, Arita N, Nomura T, et al. Transfer of multiple
747 sclerosis into severe combined immunodeficiency mice by mononuclear cells from
748 cerebrospinal fluid of the patients. Proc Natl Acad Sci U S A. 1992 Jul;89(13):6157–61.
749 34. Nielsen TR, Rostgaard K, Askling J, Steffensen R, Oturai A, Jersild C, et al. Effects of
750 infectious mononucleosis and HLA-DRB1*15 in multiple sclerosis. Mult Scler. 2009
751 Apr;15(4):431–6.
752 35. Masterman T, Ligers A, Olsson T, Andersson M, Olerup O, Hillert J. HLA-DR15 is
753 associated with lower age at onset in multiple sclerosis. Ann Neurol. 2000
754 Aug;48(2):211–9.
755 36. Mohme M, Hotz C, Stevanovic S, Binder T, Lee J-H, Okoniewski M, et al. HLA-DR15-
756 derived self-peptides are involved in increased autologous T cell proliferation in
757 multiple sclerosis. Brain. 2013 Jun;136(Pt 6):1783–98.
758 37. Jelcic I, Al Nimer F, Wang J, Lentsch V, Planas R, Jelcic I, et al. Memory B Cells Activate
759 Brain-Homing, Autoreactive CD4(+) T Cells in Multiple Sclerosis. Cell. 2018/09/04.
760 2018;175(1):85-100.e23.
761 38. Zdimerova H, Murer A, Engelmann C, Raykova A, Deng Y, Gujer C, et al. Attenuated
762 immune control of Epstein-Barr virus in humanized mice is associated with the
763 multiple sclerosis risk factor HLA-DR15. Eur J Immunol. 2021 Jan;51(1):64–75.
764 39. Bjornevik K, Cortese M, Healy BC, Kuhle J, Mina MJ, Leng Y, et al. Longitudinal analysis
765 reveals high prevalence of Epstein-Barr virus associated with multiple sclerosis.
766 Science. 2022 Jan;375(6578):296–301.
767 40. Sundström P, Nyström M, Ruuth K, Lundgren E. Antibodies to specific EBNA-1
768 domains and HLA DRB1*1501 interact as risk factors for multiple sclerosis. J
769 Neuroimmunol. 2009 Oct;215(1–2):102–7.
770 41. Lanz T V, Brewer RC, Ho PP, Moon J-S, Jude KM, Fernandez D, et al. Clonally expanded
771 B cells in multiple sclerosis bind EBV EBNA1 and GlialCAM. Nature. 2022
772 Mar;603(7900):321–7.

773 42. Tengvall K, Huang J, Hellström C, Kammer P, Biström M, Ayoglu B, et al. Molecular
774 mimicry between Anoctamin 2 and Epstein-Barr virus nuclear antigen 1 associates
775 with multiple sclerosis risk. Proc Natl Acad Sci U S A. 2019 Aug;116(34):16955–60.
776 43. Hecker M, Fitzner B, Wendt M, Lorenz P, Flechtner K, Steinbeck F, et al. High-Density
777 Peptide Microarray Analysis of IgG Autoantibody Reactivities in Serum and
778 Cerebrospinal Fluid of Multiple Sclerosis Patients. Mol Cell Proteomics. 2016
779 Apr;15(4):1360–80.
780 44. Jog NR, McClain MT, Heinlen LD, Gross T, Towner R, Guthridge JM, et al. Epstein Barr
781 virus nuclear antigen 1 (EBNA-1) peptides recognized by adult multiple sclerosis
782 patient sera induce neurologic symptoms in a murine model. J Autoimmun. 2020
783 Jan;106:102332.
784 45. Yednock TA, Cannon C, Fritz LC, Sanchez-Madrid F, Steinman L, Karin N. Prevention of
785 experimental autoimmune encephalomyelitis by antibodies against alpha 4 beta 1
786 integrin. Nature. 1992 Mar;356(6364):63–6.
787 46. Tapeinou A, Androutsou ME, Kyrtata K, Vlamis-Gardikas A, Apostolopoulos V,
788 Matsoukas J, et al. Conjugation of a peptide to mannan and its confirmation by tricine
789 sodium dodecyl sulfate-polyacrylamide gel electrophoresis. Anal Biochem.
790 2015/06/17. 2015;485:43–5.
791
792
793

794 **Table 1**

795

Genotype **Diagnosis**	**G**	**Age**	**MS duration (y)**	**Therapies**	**Relapse (12/24 m)**	**MRI Brain/Gd**	**MRI Spine/Gd**	**EDSS**	**Viral infections (titre)**	**T cell responses (21)**
DR13 1302/1303 RRMS	F	42	27	Azathioprine Interferon beta-1a Interferon beta-1b Fingolimod Natalizumab (#5) Cortisone (1 m prior to sampling)	1/1	(+) stable	(+) GD (+)	2.5	**CoV2**$^{+}$ **JC**$^{+}$ (1.24) **EBV** VCA IgG^{+} **EBV** EA IgG^{+} **EBV** EBNA1 IgG^{+} **EBV** EBNA1 IgM^{-}	MBP83-99 hMOG35-55 (Patient 17)
DR15 0402/1501 RRMS	F	38	15	Interferon beta-1a Fingolimod Natalizumab (#24) Cladribine	1/1	(+) stable	(+) stable	2.5	**CoV2**$^{+}$ **JC**$^{+}$ (1.47) **EBV** VCA IgG^{+} **EBV** EA IgG^{-} **EBV** EBNA1 IgG^{+} **EBV** EBNA1 IgM^{+}	MBP13-32 MBP83-99 hMOG35-55 (Patient 11)
DR15 04/15 Healthy	F	28	None	None	None	ND	ND	ND	**CoV2**$^{+}$ **JC** ND **EBV** VCA IgG^{+} **EBV** EA IgG^{+} **EBV** EBNA1 IgG^{+} **EBV** EBNA1 IgM^{+}	None (Normal 1)

796

797 KEY: EDSS, expanded disability status scale; Gd, gadolinium; NA, not applicable; ND, not done; RRMS, relapse-remitting MS.

798

799 **Figure legends**

800

801 **Figure 1**

802 **Reconstitution of a human adaptive immune system in B2m-NOG mice engrafted with**
803 **PBMC from MS patient and healthy donors. (A)** Progressive engraftment of human (h)
804 CD45+ leukocytes from donors in groups of B2m-NOG mice, non-immunized (left) and
805 immunized using an EAE protocol (right), measured in peripheral blood samples taken at
806 different time points, and in spleen recovered at sacrifice 42 days post-transplantation (dpt
807 42). **(B)** Proportions of $hCD4^+$ and $hCD8^+$ T cells in blood $hCD45^+CD3^+$ T cells at different time
808 points. **(C)** Proportions of human immune cell subpopulations in spleens of immunized and
809 non-immunized mice at dpt 42 (see also Supplementary Table 3). **(D)** Antigen-specific T cell
810 proliferation responses to the immunizing antigens (mMOG35-55, hMOG35-55, MOG1-20,
811 MBP83-99), anti-hCD3 (positive control) and medium (unstimulated; US), in splenocytes
812 recovered from non-immunized and immunized DR13 MS PBMC humanized mice at dpt 42.
813 Results are expressed as a cell division index. **(E)** Proportions of IL-17A-producing $CD4^+$ (left
814 graph), and interferon-γ-producing (right graph) $CD4^+$ and $CD8^+$ T cells in splenocytes
815 recovered from mice in the different groups at dpt 42. **(F)** Draining lymphoid structures in
816 inguinal fat of mice engrafted with DR13 MS and DR15 MS PBMC and immunized with
817 myelin peptides, recovered at dpt 42. Immunohistochemistry revealed the presence of
818 hCD45- and mCD45-positive leukocytes, hCD4- and hCD8-positive T cells, and hCD20-
819 positive B cells (latter only DR13 MS mice). All results are depicted as mean ± SEM.
820 Statistical significance is shown after pairwise comparisons between groups using Student's
821 t test (*$p \leq 0.05$, **$p \leq 0.01$, ***$p \leq 0.001$).

822

823 **Figure 2**

824 **Human T cells accumulate at brain borders in non-immunized DR15 MS and DR15 HI mice,**
825 **and form parenchymal lesions in brain and spinal cord of DR15 MS mice**

826 Immunohistochemical analysis of the brain from non-immunized PBMC B2m-NOG mice
827 showing infiltration by human (h) and mouse (m) CD45-positive leukocytes, and hCD8-
828 positive T cells, in brain border regions (denoted in diagram **A**) and in brainstem
829 parenchyma (denoted in diagram **B**). **(B)** Parenchymal lesion containing hCD8-positive T cells

830 in brainstem of a DR15 MS mouse. **(C, D)** Accumulation of hCD45- and mCD45-positive
831 leukocytes and hCD8-positive T cells, together with local activation of Iba1-positive microglia
832 and GFAP-positive astrocytes, at border regions in the brains of DR15 HI and DR15 MS mice,
833 specifically in the connective tissue of the interventricular foramen joining the lateral and
834 third ventricles (C, arrowheads), and at meninges close to the optic tract (D, arrowheads).
835 Scattered hCD45-positive leukocytes and hCD8 T cells in brain parenchyma of DR15 MS mice
836 (C, arrows). (**E)** Counting of barrier-associated and parenchymal hCD8-positive T cells in
837 whole coronal sections of brain (shown in A) from DR13 MS, DR15 MS and DR15 HI mice.
838 Scale bar 100 µm; x20 objective (C, D). All results are depicted as mean ± SEM. Statistical
839 analysis was performed by pairwise comparisons between different groups of mice using
840 Student's t test.
841
842 **Figure 3**
843 **Human T cells infiltrate spinal cord white matter in non-immunized DR15 MS and DR15 HI**
844 **mice, and form grey matter lesions in DR15 MS mice**
845 Immunohistochemical analysis of spinal cord from non-immunized PBMC B2m-NOG mice
846 showing infiltration by human (h) CD3-positive T cells in the grey and white matter regions.
847 **(A)** Infiltrating hCD3-positive T cells were scattered individually throughout spinal cord grey
848 and white matter and formed small lesions in the white matter (WM) of both DR15 MS and
849 DR15 HI mice (lower panels, arrowheads), and grey matter lesions only in DR15 MS mice
850 (upper panels, arrowheads). The dotted lines mark the boundary between grey matter and
851 white matter. **(B)** Counting of hCD3-positive T cell lesions (≥ 3 adjacent cells) in grey and
852 white matter in whole spinal cord sections from DR15 HI and DR15 MS mice. **(C)** Semi-
853 quantitative estimation of hCD3-positive T cells in whole spinal cord sections from DR15 HI
854 and DR15 MS mice. **(D)** Double immunofluorescence staining for hCD45-positive leukocytes
855 (green, arrowheads) and MBP-positive myelin (red), with DAPI counterstained nuclei (blue),
856 in spinal cord white matter (WM) of DR15 MS mice. Grey matter (GM). Scale bars 100 µm;
857 x20 objective (A, upper panels); x40 objective (A, lower panels). All results are depicted as
858 mean ± SEM. Statistical analysis was performed by pairwise comparisons between different
859 groups of mice using Student's t test.
860
861 **Figure 4**

862 **Immunization with myelin peptides increases T cell infiltration of brain parenchyma and**
863 **promotes development of brain lesions in both DR15 MS and DR15 HI mice**
864 Immunohistochemical analysis of the brain from PBMC B2m-NOG mice immunized for EAE
865 showing infiltration by human (h) and mouse (m) CD45-positive leukocytes, hCD8- and
866 hCD4-positive T cells, and local activation of Iba1-positive microglia and GFAP-positive
867 astrocytes, in brain regions denoted in the diagram **(A)**. **(B, C)** Individual hCD45-positive
868 leukocytes and hCD8-positive T cells scattered in the corpus callosum white matter (B) and
869 small lesions in the optic tract (C, arrowhead) in the presence of locally activated Iba1-
870 positive microglia and GFAP-positive astrocytes in immunized DR15 HI mice. **(D)** Prominent
871 lesions in the corpus callosum white matter of two of the three DR15 MS mice **(i, ii,**
872 arrowheads), containing hCD45- and mCD45-positive leukocytes, hCD4- and hCD8-positive T
873 cells and locally activated Iba1-positive microglia and GFAP-positive astrocytes. **(E)** Counting
874 of barrier-associated and parenchymal hCD8-positive T cells in whole coronal sections of
875 brain from DR13 MS, DR15 MS and DR15 HI mice. **(F)** Double immunofluorescence staining
876 for hCD45-positive leukocytes (green, arrowhead) and Iba1-positive microglia/border
877 macrophages (red, yellow arrowhead; non-specific red staining of erythrocytes in vessel
878 lumen), with DAPI counterstained nuclei (blue), showing a small perivascular lesion in the
879 thalamus grey matter (GM) of immunized DR15 MS mice. **(G)** Double immunofluorescence
880 staining for hCD45-positive leukocytes (green, arrowheads) and MBP-positive myelin (red),
881 with DAPI counterstained nuclei (blue), in corpus callosum in immunized DR15 MS mice,
882 showing inflammatory lesion without demyelination. Scale bars 100 µm; x20 objective (B, C,
883 D, G); x40 objective (F). All results are depicted as mean ± SEM. Statistical analysis was
884 performed by pairwise comparisons between different groups of mice using Student's t test.
885
886 **Figure 5**
887 **Immunization with myelin peptides induces T cell lesions in spinal cord white matter of**
888 **both DR15 MS and DR15 HI mice**
889 Immunohistochemical analysis of spinal cord from PBMC B2m-NOG mice immunized for EAE
890 showing infiltration by human (h) CD3-positive T cells in the grey and white matter regions.
891 **(A)** Infiltrating hCD3-positive T cells scattered throughout spinal cord grey and white matter
892 and forming small lesions in the white matter (WM) of both DR15 MS and DR15 HI mice
893 (lower panels, arrowheads) The dotted lines mark the boundary between grey matter and

894 white matter. **(B)** Counting of hCD3-positive T cell lesions (≥ 3 adjacent cells) in grey and
895 white matter in whole spinal cord sections from DR15 HI and DR15 MS mice. **(C)** Double
896 immunofluorescence staining for hCD45-positive leukocytes (green, arrowheads) and MBP-
897 positive myelin (red), with DAPI counterstained nuclei (blue), in white matter (WM) of
898 immunized DR15 MS spinal cord. Grey matter (GM). **(D)** Semi-quantitative estimation of
899 hCD3-positive T cells in whole spinal cord sections from DR15 HI and DR15 MS mice. All
900 results are depicted as mean ± SEM. Scale bars 100 µm; x40 objective (A). Statistical analysis
901 was performed by pairwise comparisons between different groups of mice using Student's t
902 test.

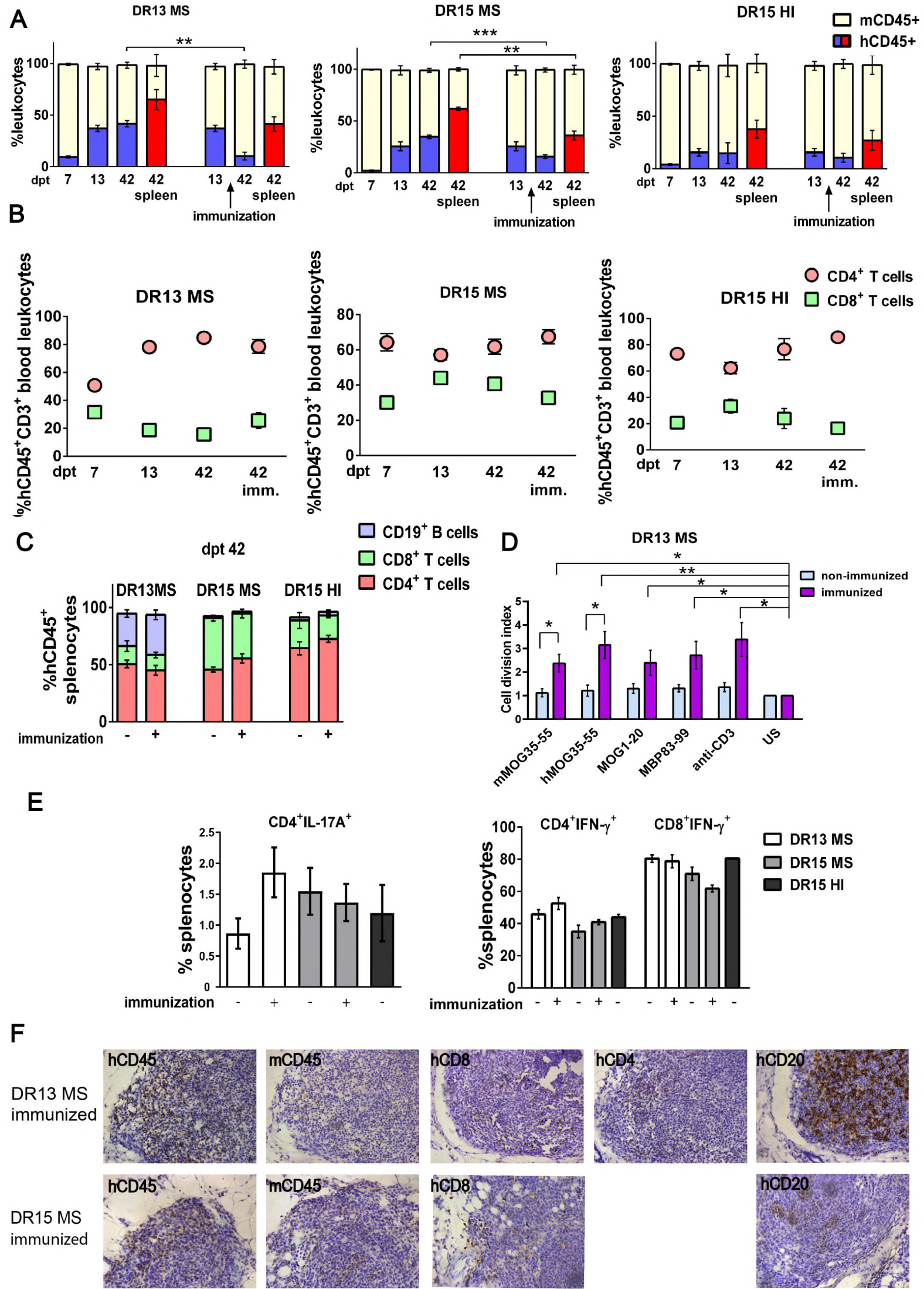
A
DR13 MS
DR15 MS
DR15 HI
mCD45+
hCD45+
%leukocytes
dpt 7 13 42 42 13 42 42
spleen
immunization
B
DR13 MS
DR15 MS
DR15 HI
CD4+ T cells
CD8+ T cells
%hCD45+CD3+ blood leukocytes
dpt 7 13 42 42
imm.
C
dpt 42
CD19+ B cells
CD8+ T cells
CD4+ T cells
DR13MS
DR15 MS
DR15 HI
%hCD45+ splenocytes
immunization - + - + - +
D
DR13 MS
non-immunized
immunized
Cell division index
mMOG35-55
hMOG35-55
MOG1-20
MBP83-99
anti-CD3
US
E
CD4+IL-17A+
% splenocytes
CD4+IFN-γ+
CD8+IFN-γ+
%splenocytes
DR13 MS
DR15 MS
DR15 HI
immunization - + - + -
F
DR13 MS immunized
DR15 MS immunized
hCD45
mCD45
hCD8
hCD4
hCD20

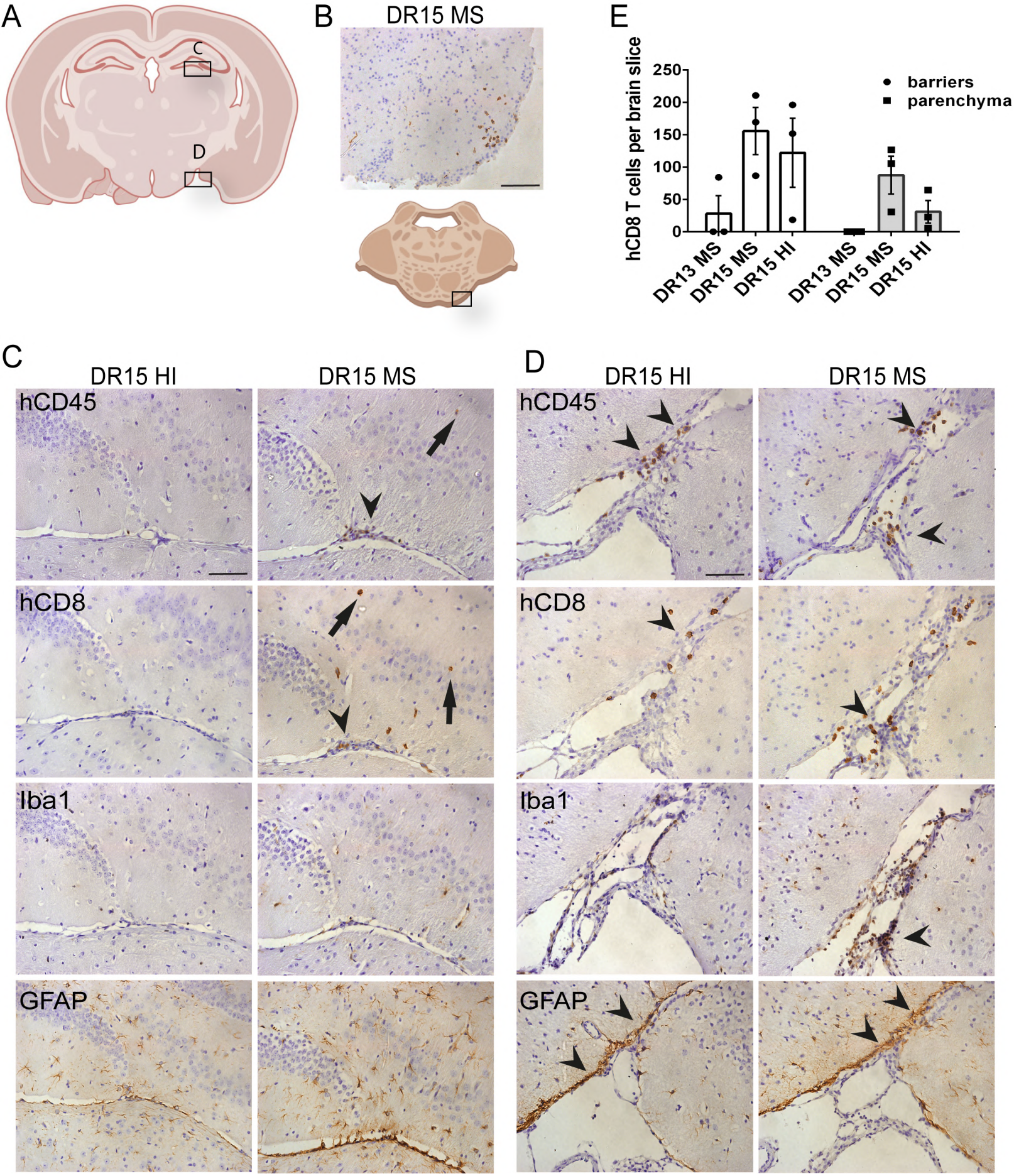
A
C
D
B
DR15 MS
E
hCD8 T cells per brain slice
250
200
150
100
50
0
barriers
parenchyma
DR13 MS
DR15 MS
DR15 HI
DR13 MS
DR15 MS
DR15 HI
C
DR15 HI
DR15 MS
hCD45
hCD8
Iba1
GFAP
D
DR15 HI
DR15 MS
hCD45
hCD8
Iba1
GFAP

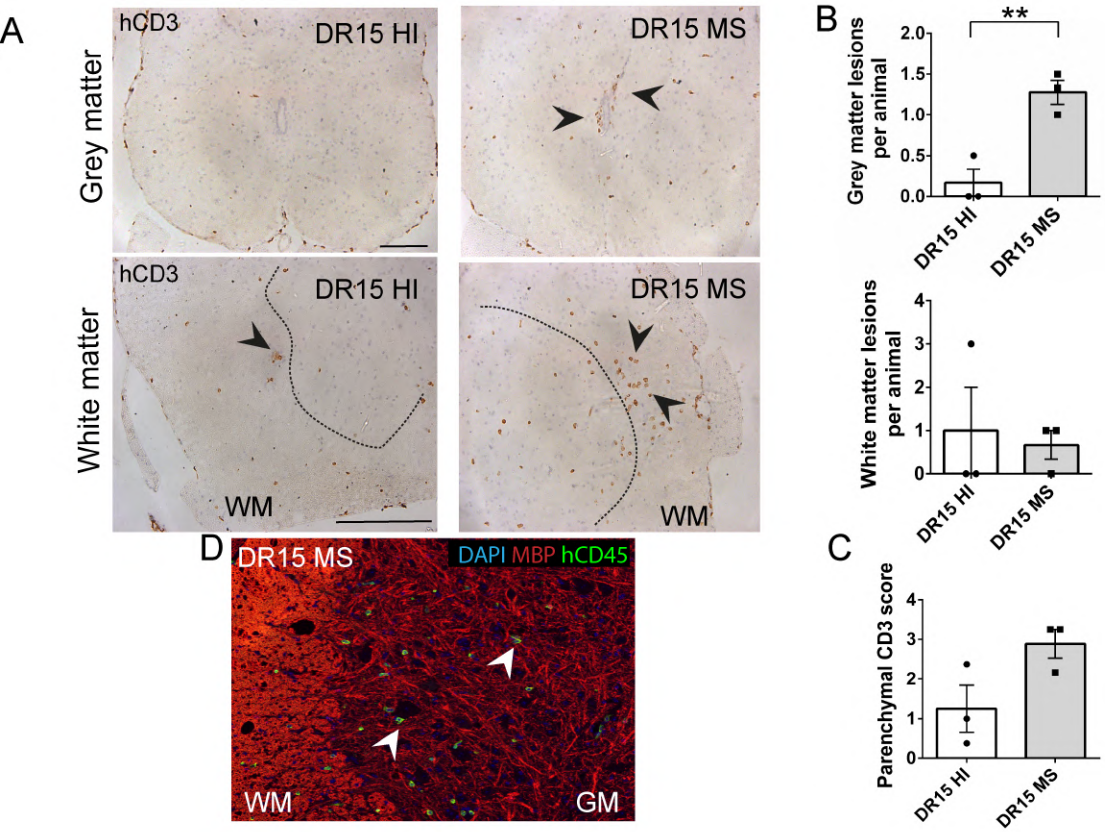
A
hCD3
DR15 HI
DR15 MS
Grey matter
White matter
WM
B
**
Grey matter lesions per animal
2.0
1.5
1.0
0.5
0.0
DR15 HI
DR15 MS
White matter lesions per animal
4
3
2
1
0
C
Parenchymal CD3 score
D
DAPI MBP hCD45
GM

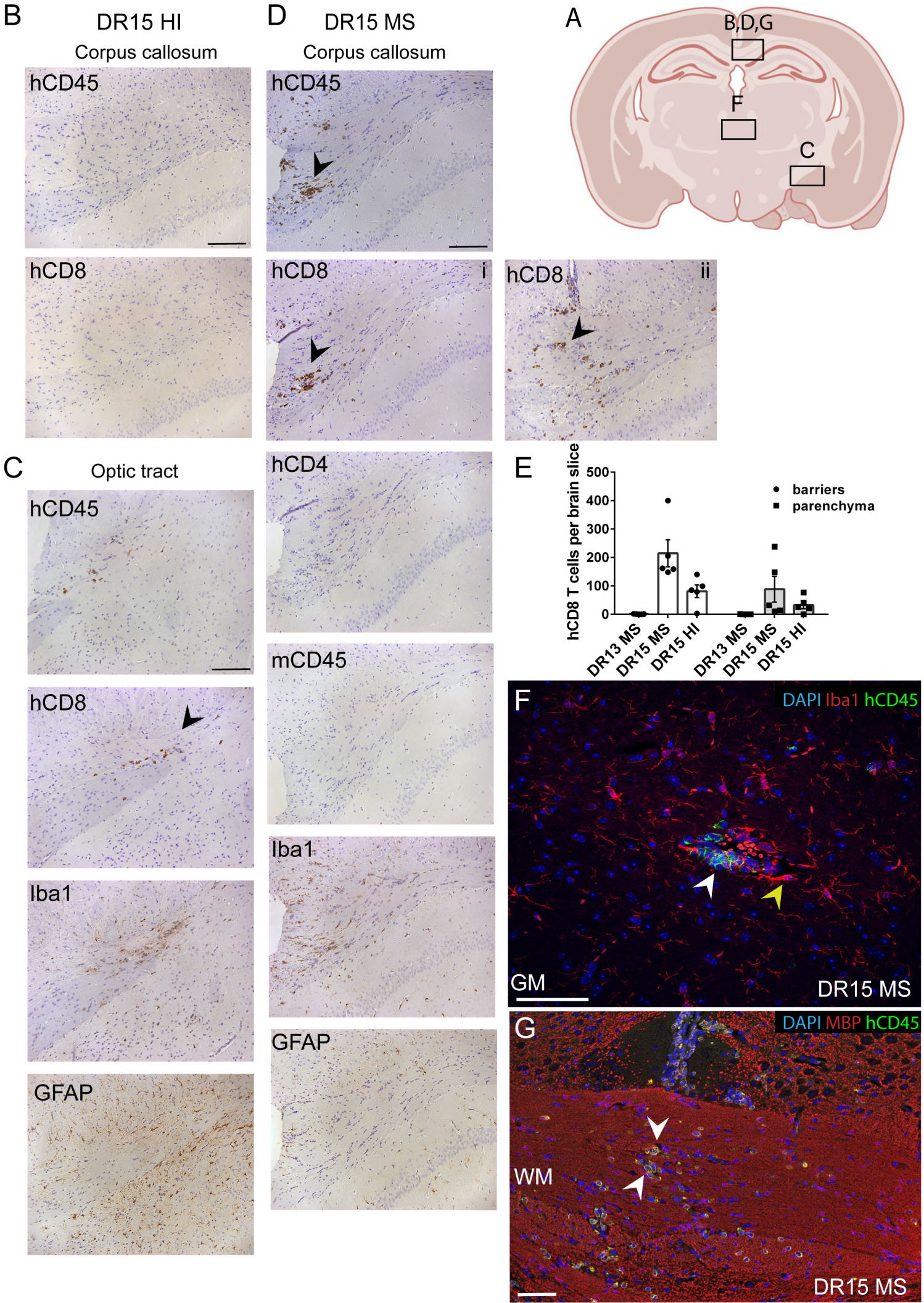
B
DR15 HI
Corpus callosum
hCD45
hCD8
D
DR15 MS
Corpus callosum
hCD45
hCD8
i
hCD8
ii
A
B,D,G
F
C
C
Optic tract
hCD45
hCD8
Iba1
GFAP
hCD4
mCD45
Iba1
GFAP
E
hCD8 T cells per brain slice
500
400
300
200
100
0
barriers
parenchyma
DR13 MS
DR15 MS
DR15 HI
DR13 MS
DR15 MS
DR15 HI
F
DAPI Iba1 hCD45
GM
DR15 MS
G
DAPI MBP hCD45
WM
DR15 MS

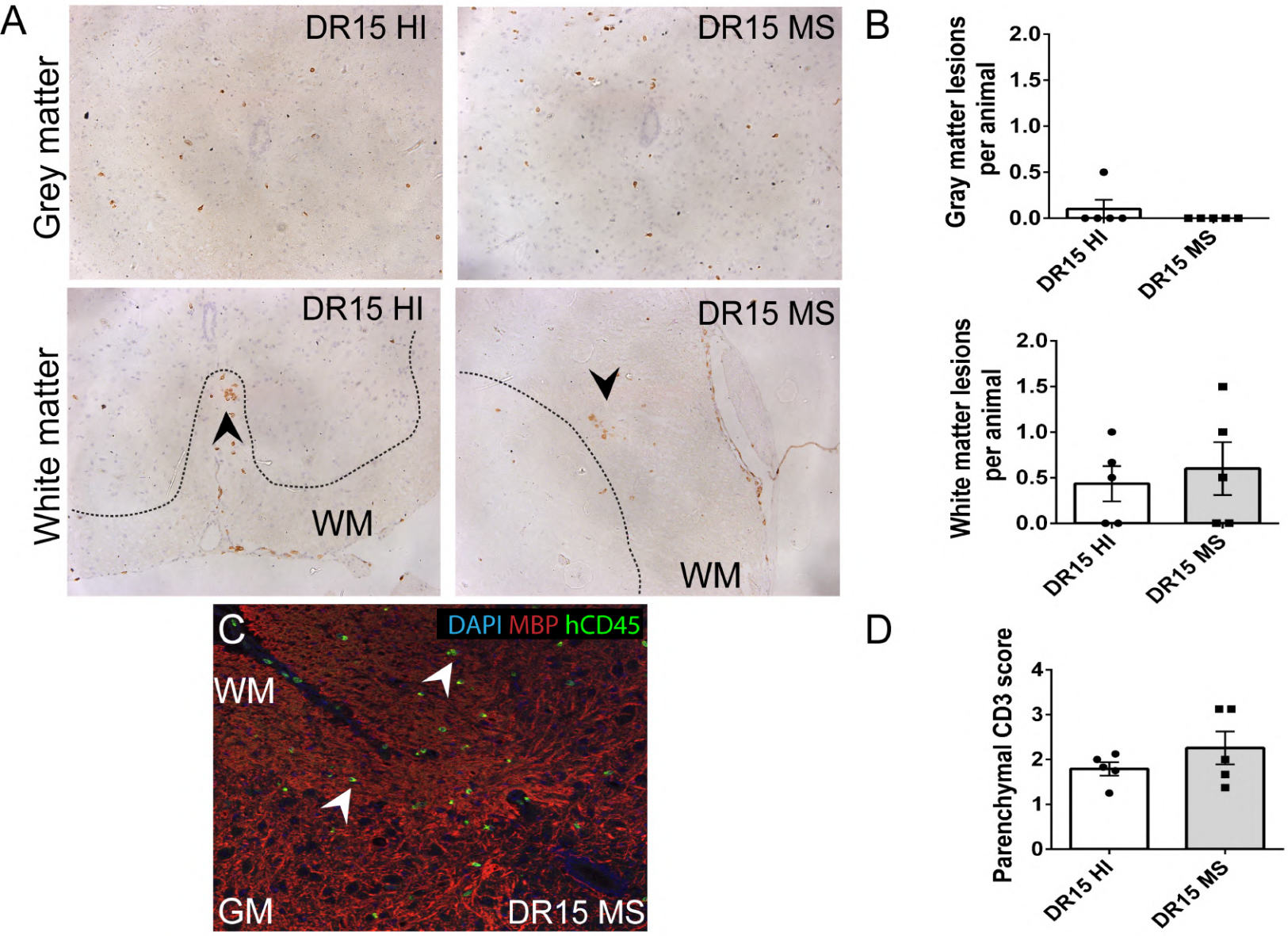
A
Grey matter
DR15 HI
DR15 MS
White matter
DR15 HI
DR15 MS
WM
WM
B
Gray matter lesions per animal
2.0
1.5
1.0
0.5
0.0
DR15 HI
DR15 MS
White matter lesions per animal
2.0
1.5
1.0
0.5
0.0
DR15 HI
DR15 MS
C
DAPI MBP hCD45
WM
GM
DR15 MS
D
Parenchymal CD3 score
4
3
2
1
0
DR15 HI
DR15 MS